The 5th Joint International Conference on Multibody System Dynamics
June 24 – 28, 2018, Lisboa, Portugal

Using superposition of local soil flow fields to improve soil deformation in the DLR Soil Contact Model - SCM

Fabian Buse[1]
[1] *Institue of System Dynamics and Control, German Aerospace Center (DLR), fabian.buse@dlr.de*

ABSTRACT — *Locomotion on soft sandy soil poses high risks to planetary rovers. Especially events like the embedding of* SPIRIT *emphasize these risks. Since scientifically interesting regions may be in or behind sandy areas, tools to predict locomotion on this terrain are important. To evaluate motion on a sandy terrain a simulation of the full system with a capable terramechanical model is needed. The Soil Contact Model - (SCM) was developed with the goal of incorporating effects induced by soil deformation like rutting and slip sinkage into a multi body environment. This paper presents a novel approach to the soil deformation algorithm in SCM.*

1 Introduction

In order to ensure a safe operation of a planetary rover many aspects have to be considered. One being the locomotion. The traversal of sandy areas poses a great risk to a rover. This was emphasized by the entrapment of the rover SPIRIT [1] or CURIOSITY's traversal of sand ripples near gale crater [2]. This leads to the requirement of a thorough understanding of the interaction between wheels and sand. To analyze the process at hand different approaches are possible. Physical testing with rover prototypes [3] or with testbeds as shown in [4] are a viable choice. These experiments provide accurate results but are limited to specific conditions and environments. To counteract those drawbacks simulations are well suited. Terramechanical simulations can be grouped by their purpose.

Simulations using discrete element models are typically used for a detailed analysis of a specific aspect. For example in the design of a wheel [5]. These types of simulations are computational complex and thus the application use for full system analysis is limited. Simulations based on empirical models are usually faster but do not depict all effects and are thus less precise. These models are usually used to analyze or predict the behavior of a full system. As applied in Artemis [6] or in the DLR Rover Simulation Toolkit [7], Figure 1 shows an exemplary

Fig. 1: Full rover simulation with the DLR Rover Simulation Toolkit using SCM. The shown scenario is used in Section 4.3 to qualitatively show the capabilities of rover locomotion simulation in SCM

application of the RST with DLR Soil Contact Model (SCM). By explicitly modeling the effects of soil deformation in SCM, its capabilities are greatly enhanced. The influence of soil deformation is usually modeled implicitly in the force laws [8] or approximated by introducing elastoplastic effects as in [9]. In this paper a novel approach to cover the soil deformation in SCM is discussed.

2 Soil Contact Model (SCM) - A contact model for use in a multibody system

SCM is a terramechanical model with the purpose of being used in a multi body simulation environment and was first presented by KRENN in 2008 [10]. It is purposely build to depict the necessary effects needed for the simulation of rover traversing uneven sandy terrain. Internal soil process are only modeled as needed, especially effects like soil deformation and flow. As a result, SCM is able to reproduce effects such as rutting and slip sinkage and further to model other effects such as multipass due to SCM's persistent ground states. The usage scenario of kinematic analysis of a full rover poses some requirements on the model, foremost a limit to the computational complexity. The model, used in an multi body environment, should be able to simulate a rover driving a couple of meters in a couple of CPU hours.

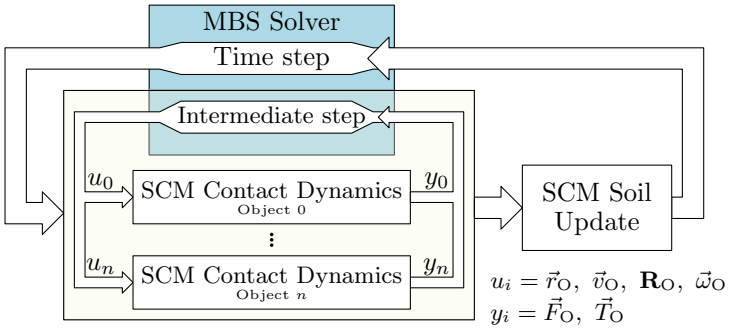

Fig. 2: Coupling of SCM to a generic multi body system solver.

SCM is a self contained C++ Library that can be coupled to any suitable simulation software. To improve SCMs performance it is divided into two major elements, see Figure 2, a contact dynamics and a soil updated step. The contact dynamics steps use the last known soil geometry in combination with the current kinematic state of the contact object to calculate the resulting forces and torques. The soil update step is either called once the solver converged or with a fixed time step. During this step the soil is deformed based on the last known kinematic states of the contact objects. A detailed description of the individual steps can be found in [11].

The soil is described as a digital elevation map. The equidistant points, further called nodes, simplify all calculations drastically. The deformation is achieved by manipulating the nodes z-coordinates. To model the soil each node is described by its position and a set of additional states, like soil flow velocity or flow volume. These states are updated in conjunction with the deformation.

3 Soil Deformation in SCM

The main element of SCM is an efficient description of the soil deformation. Each node in contact i_c displaces a volume of soil $V_\zeta(i_c)$ defined by the overlap between the contact objects lowest point $z_{\text{Obj}}(i_c)$ at the node and the vertical component of the nodes position $\vec{r}(i_c)$. The area A_{Grid} is constant for all nodes and directly results from the resolution (d_x, d_y) of the elevation map.

$$A_{\text{Grid}} = d_x d_y \tag{1}$$

$$V_\zeta(i_c) = \max\left(\vec{e}_z \cdot \vec{r}(i_c) - z_{\text{Obj}}(i_c), 0\right) A_{\text{Grid}} \tag{2}$$

The soil deformation formulation has to move this displaced volume from the displacing node (i_c) to other, surrounding nodes (i_δ). The previously used soil deformation algorithm, see [10, 11] for a detailed description, was

Fig. 3: Particle image velocimetry (PIV) [13, 14] used as reference during the development of new algorithm. PIV images provided by NASA/JPL/Carnegie Mellon University.

based on the concept that the displaced volume is initially distributed onto the border nodes and then deposited further onto nodes that are not in contact. This formulation had the benefit of being robust and fast. In the original implementation, only an erosion algorithm was used to further deposit the soil from the border nodes. The extensions introduced in [11] improved the process by introducing two separate internal procedures for sheared and compressed soil. With this algorithm adequate results were possible. However, since neither the original nor the extended algorithm considered nodes between a contact node and a border node, both showed limitations in application with non smooth contact objects. This drawback especially occurs in the case of a wheel with grousers. To counteract this drawback and to improve the quality of the model a completely new algorithm was developed.

The new algorithm is based on five assumptions which simplify the soil flow process and make it possible to implement it in SCM. The assumptions are derived from theoretical soil mechanics, notably by RANKINE failure criterion [12, pp. 246–248] as well as particle image velocimetry (PIV) data from experiments, as shown in Fig. 3.

First assumption: The global flow field induced by an object displacing soil can be approximated by super positioning local flow fields that are calculated for each single point in contact independently.

Second assumption: The flow field induced by a single contact point can be described by the states of that point and the previous states of all other points.

Third assumption: Flow velocity at each contact point is equal to the velocity of the body displacing the soil. This assumption is based on the idea that the flow is only initiated because the soil volume was displaced by the object, and thus has locally assumed the velocity of that object.

Fourth assumption: Uninfluenced shear failure in a flow field propagates along the sliding surfaces from the RANKINE's active or passive state. Which sliding surface is used at a certain point i.e. active or passive, depends on the direction of flow induced by the local flow field and the flow velocity that was calculated previously at this point. If local and previously calculated flow align the passive sliding surface is used, otherwise the active sliding surface is applied.

Fifth assumption: Flow will propagate downwards when the surface is loaded and propagates upwards when the surface is free of load.

Based on assumption one and two, an individual, local, flow field for each node can be calculated based on its current and the previous states of all other nodes independently. This allows avoiding solving an equilibrium and thus greatly reduce the computational complexity. The local flow fields are spanned by applying the assumptions three to five to discrete directions, further called chords. Each chord is a 2D representation of the resulting flow. This approach is a consequence of the requirement of low computational effort which opposes a global formulation. In order to transfer the information from the chords to all nodes, an interpolation is applied in a second step. This method efficiently generates the local flow fields. These local fields are then superimposed based on assumption two to generate one global flow field.

A flow field in SCM is described by three variables. The flow depth h_δ, or depth of shear failure, describing the geometric depth interface between moving and unaffected soil, the volumetric soil flow $\vec{Q}_\delta$ describing the

directional flow of soil that is flowing through the a node and the volume of soil that V_δ is deposited onto a specific node.

To compute these three variables a set of auxiliary variables is calculated on each chord. Which are used to define the local flow field and are combined further to be super positioned to generate the final field.

3.1 Soil deformation algorithm

A set of n_C chords is constructed for every node displacing soil. Each chord, indexed by (k_C), is defined by the vertical axis $\vec{e}_z$ and a directional vector $\vec{e}_\mathrm{C}(k_\mathrm{C})$. To prevent unwanted directional effects the whole chord set is randomly rotated by α_RND.

$$\alpha_\mathrm{C}(k_\mathrm{C}) = 2\,\pi\frac{k_\mathrm{C}}{n_\mathrm{C}} + \alpha_\mathrm{RND} \tag{3}$$

$$\vec{e}_\mathrm{C}(k_\mathrm{C}) = \begin{pmatrix} \sin(\alpha_\mathrm{C}(k_\mathrm{C})) \\ \cos(\alpha_\mathrm{C}(k_\mathrm{C})) \\ 0 \end{pmatrix} \tag{4}$$

One chord describes how an amount of soil, that is displaced at the origin, would move and deform the soil in

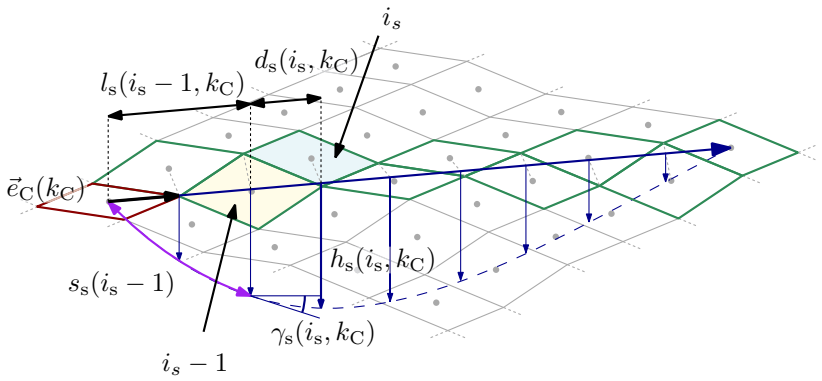

Fig. 4: Sketch visualizing the calculation of the flow depth $h_\mathrm{s}(i_\mathrm{s})$ on a chord based on the previous depth $h_\mathrm{s}(i_\mathrm{s}-1)$ and the current propagation angle $\gamma_\mathrm{s}(i_\mathrm{s})$.

this direction. Hence the failure propagation starts at the contact node in the center and then propagates along the direction $\vec{e}_\mathrm{C}$. For each node i_s on the chord the local flow depth h_s, the shear length s_s, the distance to the center l_s as well as the propagation angle γ_s are calculated. As shown in Fig. 4, the flow depth at a node is calculated from the current propagation angle, the previous propagation depth and the horizontal distance d_s between the nodes. The values in Fig. 4 are calculated as follows:

$$d_\mathrm{s} = |(r(i_\mathrm{s}) - r(i_\mathrm{s}-1)) \cdot \vec{e}_\mathrm{C}(k_\mathrm{C})| \tag{5}$$

$$l_\mathrm{s}(i_\mathrm{s}, k_\mathrm{C}) = l_\mathrm{s}(i_\mathrm{s}-1, k_\mathrm{C}) + d_\mathrm{s} \tag{6}$$

$$h_\mathrm{s}(i_\mathrm{s}, k_\mathrm{C}) = h_\mathrm{s}(i_\mathrm{s}-1, k_\mathrm{C}) + d_\mathrm{s}\,\tan(\gamma(i_\mathrm{s}, k_\mathrm{C})) \tag{7}$$

$$s_\mathrm{s}(i_\mathrm{s}, k_\mathrm{C}) = s_\mathrm{s}(i_\mathrm{s}-1, k_\mathrm{C}) + \frac{d_\mathrm{s}}{\cos(\gamma(i_\mathrm{s}, k_\mathrm{C}))} \tag{8}$$

According to assumption three, the initial propagation angle $\bar{\gamma}$ is directly based upon the contact velocity and is bounded by within $[-\gamma_a, \gamma_a]$ the propagating angle in the active failure state.

$$\gamma_a = \frac{\pi}{4} + \frac{\phi}{2} \tag{9}$$

$$\bar{\gamma}_\mathrm{s}(k_\mathrm{C}) = \mathrm{atan2}\left(\vec{v}_\mathrm{c}(i_\mathrm{c}) \cdot \vec{e}_z, \vec{v}_\mathrm{c}(i_\mathrm{c}) \cdot \vec{e}_\mathrm{C}(k_\mathrm{C})\right) \tag{10}$$

$$\gamma_\mathrm{s}(i_\mathrm{s}=0,k_\mathrm{C}) = \begin{cases} -\gamma_a & \forall \quad \bar{\gamma}_\mathrm{s}(k_\mathrm{C}) \leq -\gamma_a \\ \bar{\gamma}_\mathrm{s}(k_\mathrm{C}) & \forall -\gamma_a < \bar{\gamma}_\mathrm{s}(k_\mathrm{C}) < \gamma_a \\ \gamma_a & \forall \quad \gamma_a \leq \bar{\gamma}_\mathrm{s}(k_\mathrm{C}) \end{cases} \tag{11}$$

Derived from assumption five, the propagation angle $\tilde{\gamma}$ at a node that is not influenced by any previous node is dependent on the load situation and on the relationship between the already active soil flow at the node and the directional flow that would be generated by this chord. If there is load on the node the sign of $\tilde{\gamma}_\mathrm{s}$ is defined to be negative else $\tilde{\gamma}_\mathrm{s}$ is positive. The distinction between loaded and unload nodes can be simplified to the distinction if a node is in contact or not. This simplification is equal to the initially designed assumption since all nodes in contact will experience load.

$$\mathrm{sign}\left(\tilde{\gamma}_\mathrm{s}(i_\mathrm{s})\right) = \begin{cases} -1 \; \forall \, \vec{r}(i_\mathrm{s}) \cdot \vec{e}_z \geq z_\mathrm{Obj}(i_\mathrm{s}) \\ \quad 1 \; \forall \, \vec{r}(i_\mathrm{s}) \cdot \vec{e}_z < z_\mathrm{Obj}(i_\mathrm{s}) \end{cases} \tag{12}$$

Based on assumption four, the magnitude of $\tilde{\gamma}_\mathrm{s}$ is either γ_a, if the chord direction $\vec{e}_\mathrm{C}(k_\mathrm{C})$ is opposing the soil flow $\vec{v}_\delta$ at the node, or γ_p ,if $\vec{v}_\delta$ and $\vec{e}_\mathrm{C}(k_\mathrm{C})$ are aligned.

$$\gamma_p = \frac{\pi}{4} - \frac{\phi}{2} \tag{13}$$

$$|\tilde{\gamma}_\mathrm{s}| = \begin{cases} \gamma_p & \forall \, \vec{e}_\mathrm{C}(k_\mathrm{C}) \cdot \vec{v}_\delta \geq 0 \\ \gamma_a & \forall \, \vec{e}_\mathrm{C}(k_\mathrm{C}) \cdot \vec{v}_\delta < 0 \end{cases} \tag{14}$$

The uninfluenced angle $\tilde{\gamma}_\mathrm{s}$ and the angle at the previous node $\gamma_\mathrm{s}(i_\mathrm{s}-1)$ are combined with the factor λ to calculate the active propagation angle $\gamma_\mathrm{s}(i)$. The factor λ is based on the shear length and a parameter Ψ_Shape.

$$\lambda = \exp\left(-\frac{s_\mathrm{s}(i_\mathrm{s}-1,k_\mathrm{C})}{\Psi_\mathrm{Shape}}\right) \tag{15}$$

$$\gamma_\mathrm{s}(i_\mathrm{s}) = \lambda\,\gamma_\mathrm{s}(i_\mathrm{s}-1) + (1-\lambda)\tilde{\gamma}_\mathrm{s}(i_\mathrm{s}) \tag{16}$$

How quick the propagation angle aligns with the uninfluenced angle $\tilde{\gamma}_\mathrm{s}$ can be adjusted by Ψ_Shape. The described algorithm is repeated until the flow depth crosses the soil surface. The number of nodes on a chord is n_s. The length of the chord l_C is equal to the distance from of the last node to the chord origin. To calculate the distribution of soil volume in between the chords as well as on the cords, weighting factors are utilized. The first directional factor $f_\mathrm{C}(k_\mathrm{C})$ is calculated once for each chord and models the directional difference of soil flow depending on the angle between contact velocity $v_\mathrm{c}(i_\mathrm{c})$ and the respective chord direction $\vec{e}_\mathrm{C}(k_\mathrm{C})$:

$$f_\mathrm{C}(k_\mathrm{C}) = \left[\frac{\left[\max\left(\vec{v}_\delta(i_\mathrm{c})\,\vec{e}_\mathrm{C}(k_\mathrm{C}),0\right)\right]^2 + \left[\vec{v}_\delta(i_\mathrm{c})\,\vec{e}_z\right]^2}{|\vec{v}_\delta(i_\mathrm{c})|}\right]^{\Psi_\mathrm{Angle}} \tag{17}$$

This factor approaches one if the soil flow is in direction of the chord and zero if this flow is perpendicular or opposed to the chord direction. The transition between these two points is adjusted using the parameter Ψ_Angle.

The factor $\bar{f}_\mathrm{s}(i_\mathrm{s},k_\mathrm{C})$ describes the fraction of material deposited on a specific node in relation to the total deposited soil on the whole chord is calculated. This factor is assumed to follow a non-linear function of the total chord length. The non-linearity as parameterized by the parameter Ψ_Distance.

$$\bar{f}_\mathrm{s}(i_\mathrm{s},k_\mathrm{C}) = \left[\frac{d_\mathrm{s}(i_\mathrm{s})}{l_\mathrm{C}(k_\mathrm{C})}\right]^{\Psi_\mathrm{Distance}} \tag{18}$$

The final weighting factor $f_s(i_s, k_C)$ describing the relative amount associated to a node is the combination of these two factors.

$$f_s(i_s, k_C) = f_C(k_C)\, \bar{f}_s(i_s, k_C) \tag{19}$$

From f_s it is possible to calculate the relative amount of flow along a chord through one node by summing all weighting factors of following nodes. The resulting value s_s describes the relative volumetric flow through a node in relation to the displaced soil at the center node:

$$s_s(i_s, k_C) = \sum_{j=i_s+1}^{n_s} f_s(j_s, k_C) \tag{20}$$

The flow direction of the soil $\vec{t}_s$ at a node is assumed to be along the chord with the same inclination as the propagation angle:

$$\vec{t}_s(i_s, k_C) = \frac{1}{\sqrt{1+\tan(\gamma_s(i_s, k_C))^2}} \begin{pmatrix} \sin(\alpha_s(k_C)) \\ \cos(\alpha_s(k_C)) \\ \tan(\gamma_s(i_s, k_C)) \end{pmatrix} \tag{21}$$

Summarizing, the specific shape of the flow needs to be setup with the parameter Ψ_{Shape}. The quantitative soil flow is parameterized with Ψ_{Angle} and Ψ_{Distance}. Were Ψ_{Angle} influence the direction of soil flow and Ψ_{Distance} describes the distance depended distribution. All three parameters currently need to be dialed in manually, a direct derivation of those parameters from other physical soil parameters is under ongoing investigation. Currently these parameters are set by using a set of calibration scenarios described in Section 4.1.

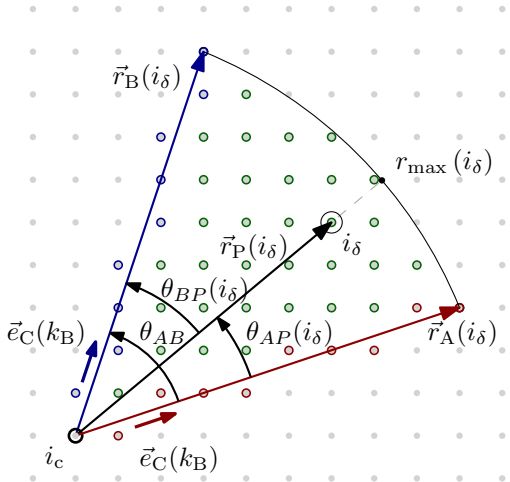

Fig. 5: interpolation sketch, red being nodes that describe chord A, blue being nodes that describe chord B and nodes in green being resulting interpolation

To transfer the localized chord information onto the full soil grid an interpolation, see Fig.5, is necessary. The applied interpolation method combines the values calculated from two chords (k_A,k_B) onto nodes enclosed by these two. Which nodes on the chords are used as reference for a specific node (i_δ) is based on the relative distance $|\vec{r}_P(i_\delta)|/r_{\max}(i_\delta)$. The relative angles, $\Theta_{AP}(i_\delta)/\Theta_{AB}$ and $\Theta_{BP}(i_\delta)/\Theta_{AB}$, between chords and the vector connecting the center node with the node in question determines how the values from the reference nodes on both chords are weighted. After the interpolation the local flow field is fully defined and for each node in this field the following states are known:

- The flow depth $h_\delta(i_c \to i_\delta)$ caused by the contact node at each node in the local flow field.
- The deposition factor $f_\delta(i_c \to i_\delta)$ describing relative volume of soil deposited at a each node in the local flow field from the contact node.
- The flow factor $s_\delta(i_c \to i_\delta)$ describing the relative volume soil flow through each node in the local flow field from the contact node.

- The flow direction $\vec{t}_\delta(i_c \to i_\delta)$ describing the direction of volumetric soil flow for each node in the local flow field from the contact node.

This set is then used to compute the absolute deposited volume soil onto a node i_δ from the contact node $V_\delta(i_c \to i_\delta)$ as well as the absolute volumetric soil flow $\vec{Q}_\delta(i_c \to i_\delta)$ through the node.

$$V_\delta(i_c \to i_\delta) = V_\zeta(i_c) \frac{f_\delta(i_c \to i_\delta)}{\sum_{i_\delta=1}^{n_\delta} f_\delta(i_c \to i_\delta)} \tag{22}$$

$$\vec{Q}_\delta(i_c \to i_\delta) = V_\zeta(i_c) \frac{\vec{t}_\delta(i_c \to i_\delta)\, s_\delta(i_c \to i_\delta)}{\sum_{i_\delta=1}^{n_\delta} f_\delta(i_c \to i_\delta)} \tag{23}$$

These are then summed over all contact nodes to calculate the final volumetric flow $\vec{Q}_\delta(i_\delta)$ and deposited volume $V_\delta(i_\delta)$ onto a node i_δ.

$$V_\delta(i_\delta) = \sum_{i_c}^{n_c} V_\delta(i_c \to i_\delta) \tag{24}$$

$$\vec{Q}_\delta(i_c \to i_\delta) = \sum_{i_c}^{n_c} \vec{Q}_\delta(i_c \to i_\delta) \tag{25}$$

$$\tag{26}$$

To calculate the final flow depth $h(i_\delta)$ at a node i_δ the flow depths calculated for that node from all contact nodes i_c are weighted with the amount of soil flow caused on the current node by the contact node:

$$h_\delta(i_\delta) = \frac{\sum_{i_c=1}^{n_c} \left(h_\delta(i_c \to i_\delta) \left| \vec{Q}_\delta(i_c \to i_\delta) \right| \right)}{\sum_{i_c=1}^{n_c} \left| \vec{Q}_\delta(i_c \to i_\delta) \right|} \tag{27}$$

The final value that is of interest for all nodes is the soil flow velocity $\vec{v}_\delta(i_\delta)$. To extract the velocity from the volumetric flow a reference area A_{Flow} needs to be defined. This area is approximated by largest intersection of the cuboid spanned by the grid (d_x, d_y) and the flow depth $h_\delta(i_\delta)$ with a plane perpendicular to the flow velocity.

$$A_{\text{Flow}}(i_\delta) = \left| \begin{pmatrix} d_x & 0 & 0 \\ 0 & d_y & 0 \\ 0 & 0 & h_\delta(i_\delta) \end{pmatrix} \frac{\vec{Q}_\delta(i_\delta)}{|\vec{Q}_\delta(i_\delta)|} \right| \tag{28}$$

$$\vec{v}_\delta(i_\delta) = \frac{\vec{Q}_\delta(i_\delta)}{A_{\text{Flow}}(i_\delta)\, dt} \tag{29}$$

To apply the calculated soil deformation to the grid, the height of each node $\vec{r}$ has to be changed according to the calculated values:

$$\vec{r}(i_\delta, t+1) = \vec{r}(i_\delta, t) + \vec{e}_z \frac{V_\delta(i_\delta) - V_\zeta(i_\delta)}{A_{\text{Grid}}} \tag{30}$$

To ensure that the angle of repose is not violated an additional erosion algorithm is applied to all nodes not in contact. The algorithm is explained in [10].

3.2 Force Calculation

The goal for the soil deformation algorithm is to provide the needed informations to calculate the resulting forces and torques acting on an object. The force law designed for SCM is based on the shear length $\vec{j}(i_c)$ which results

from the integration of the soil flow velocity $\vec{v}_\delta(i_c)$.

$$\vec{j}(i_c) = \int \vec{v}_\delta(i_c) dt \tag{31}$$

$$\vec{j}_v(i_c) = \vec{e}_z \left(\vec{j}(i_c) \cdot \vec{e}_z \right) \tag{32}$$

$$\vec{j}_h(i_c) = \vec{j}(i_c) - \vec{j}_h(i_c) \tag{33}$$

The resulting shear length is split in a vertical $\vec{j}_v(i)$ and horizontal $\vec{j}_h(i)$ component. The vertical component is used in a formulation similar to BEKKER's pressure sinkage relation [15, p. 127] with a parameter setting the soil stiffness k and a parameter setting the non-linearity n to compute the resulting normal stress at a node.

$$\vec{\sigma}(i_c) = \vec{e}_z k \left| \vec{j}_v(i_c) \right|^n \tag{34}$$

The shear stress is based on a reduction of the maximum shear stress from MOHR COULOMB's failure criterion with JANOSI HANAMOTO's shear length, shear stress reduction [15, pp. 141–143]. The parameters soil cohesion c, angle of repose ϕ, and a shear length module K define this equation. This combination is applied to the horizontal component of the shear length $\vec{j}_v(i)$ and uses the previously computed normal stress.

$$\vec{\tau}(i_c) = [c + |\vec{\sigma}(i_c)| \tan\phi] \begin{pmatrix} -\mathrm{sgn}\left(\vec{j}_v(i_c) \cdot \vec{e}_x\right) \left(1 - \exp\left(-\frac{|\vec{j}_v(i_c) \cdot \vec{e}_x|}{K}\right)\right) \\ -\mathrm{sgn}\left(\vec{j}_v(i_c) \cdot \vec{e}_y\right) \left(1 - \exp\left(-\frac{|\vec{j}_v(i_c) \cdot \vec{e}_y|}{K}\right)\right) \\ -\mathrm{sgn}\left(\vec{j}_v(i_c) \cdot \vec{e}_z\right) \left(1 - \exp\left(-\frac{|\vec{j}_v(i_c) \cdot \vec{e}_z|}{K}\right)\right) \end{pmatrix} \tag{35}$$

Combining these two to stresses to a total stress and further multiplied with the node surface area $A(i)$ the resulting force can be computed.

$$\vec{F}(i_c) = A(i_c) \left(\vec{\sigma}(i_c) + \vec{\tau}(i_c) \right) \tag{36}$$

The total reaction force and torque then calculated by summing all forces of contact nodes of the object:

$$\vec{F}_{\mathrm{Obj}} = \sum_{i_c=1}^{n_c} \vec{F}(i_c) \tag{37}$$

$$\vec{T}_{\mathrm{Obj}} = \sum_{i_c=1}^{n_c} \left(\vec{r}(i_c) - \vec{r}_{\mathrm{Obj}} \right) \times \vec{F}(i_c) \tag{38}$$

4 Experimental Results

To show that the described approach is applicable, for the simulation of an object - soil interaction, multiple aspects have to be reviewed. The two major aspects are the resulting soil flow and deformation as well as the calculated force. Validation of the generated force is mostly excluded in this work since it is topic of a current joint DLR - JPL investigation, and will be part of future publication.

4.1 Parameter Identification

To identify the SCM specific soil flow parameters Ψ_{Shape}, Ψ_{Angle} and Ψ_{Distance} two scenarios, as shown in Fig. 6 where chosen. The first scenario, shown on the left, is used to identify the first parameter Ψ_{Shape} which directly influences the shape of the induced flow field. The second scenario shown on the right is then used to identify the remaining parameters Ψ_{Angle} and Ψ_{Distance} which govern the resulting soil flow with regards to angle as well as distance dependencies.

Fig. 6: Overview on the scenarios used to validate the soil flow in SCM against. Strip load experiment on the left and the blade experiment on the right.

The strip load experiment is designed to analyze the resulting shear failure under a vertical load. The high aspect ratio simplifies the analysis, if done in the center, to infinite half-space case. By adjusting the value of Ψ_{Shape} the shape of the resulting pattern can be adjusted.

The value of Ψ_{Shape} is currently set manually by comparing of the resulting flow field and the theoretical shape from [12]. With the angle of repose set to 30.5°, similar to olivine sand, the value for Ψ_{Shape} is roughly 1.5 m. Defining this parameter to a higher precision would require a direct measurement of the flow in an experiment. With the current method only a rough approximation of $\pm 0.2\,\text{m}$ is possible. Two resulting flow fields, for a too small ($\Psi_{\text{Shape}} = 0.1\,\text{m}$) and for a too high ($\Psi_{\text{Shape}} = 10\,\text{m}$) value are shown for comparison in Fig. 7 on the bottom. The identified parameter is kept constant for all following experiments. A deviation from the theoretical result is visible directly below the load. SCM results show a much smoother shape since it results from the superposition of the individual flow fields, further investigations on this topic are planned.

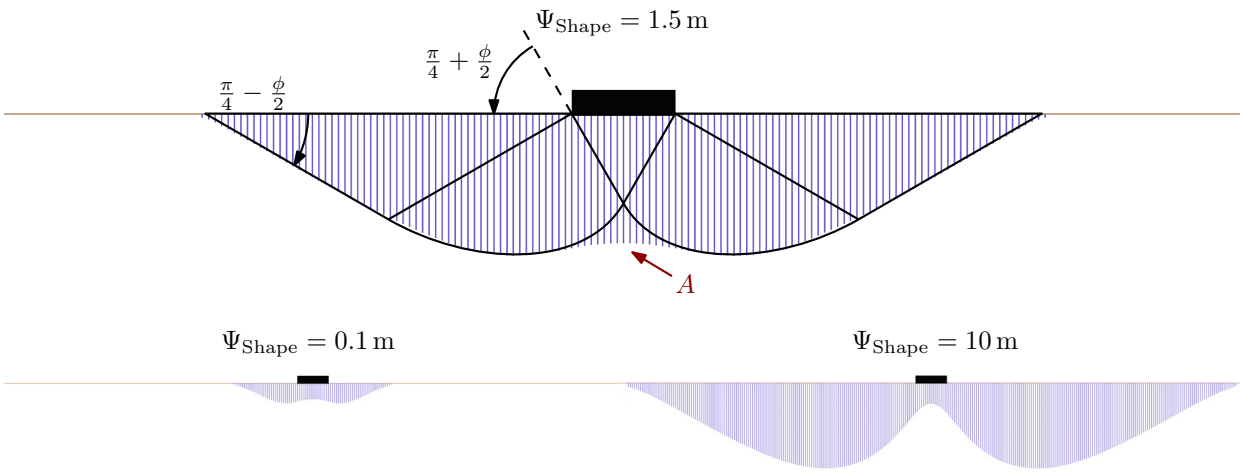

Fig. 7: Resulting shear depth under a strip load, the flow depth h_δ calculated by SCM is visualized in purple. Comparison of SCM results with a properly set $\Psi_{\text{Shape}} = 1.5\,\text{m}$ against the failure pattern under a strip load from [12] at the top. As well as two SCM with Ψ_{Shape} set to low too 0.1 m on the bottom left and Ψ_{Shape} set too high to 10 m on the bottom left.

The second experiment, the blade experiment shown in Fig. 6 on the right, is used to identify the parameters Ψ_{Angle} and Ψ_{Distance}. It is designed to compare the resulting deformation induced by a 12 cm wide blade moving horizontally through the ground. The horizontal motion is started after the blade is pushed 5 cm into the ground. To provide a better representation of the actual process in SCM the blade is titled by 5°, in both simulation and measurement. If the blade was placed vertical the nodes coming in contact would instantaneously compressed to the lower position. This would result in in an increased error.

The same scenario was executed on the Terramechanics Robotics Locomotion Lab (TROLL) to provide data for comparison. The blade was oriented and moved accordingly to the previously described setup. Thereafter the resulting resulting soil deformation in front of the blade was then captured using the laser scanner mounted on the TROLL. Figure 8 shows the experimental setup on the left and in the middle as well as the resulting surface scan

Fig. 8: Experiment to determine the parameters Ψ_{Angle} and Ψ_{Distance} using the TROLL [4]. General experiment setup shown on the left, the resulting deformation shown in the middle and the surface scan of the resulting deformation on the right

on the right.

The shape of this hill can be matched by setting the parameters Ψ_{Angle} and Ψ_{Distance} correctly. To match the shape these parameters have to be set manually. A good match can be achieved by choosing $\Psi_{\text{Angle}} = 6$ and $\Psi_{\text{Distance}} = 2$. Fig. 9 shows that the simulated deformation from SCM matches the measured surface profile. Minor deviations are still visible on the flanks and on the far end.

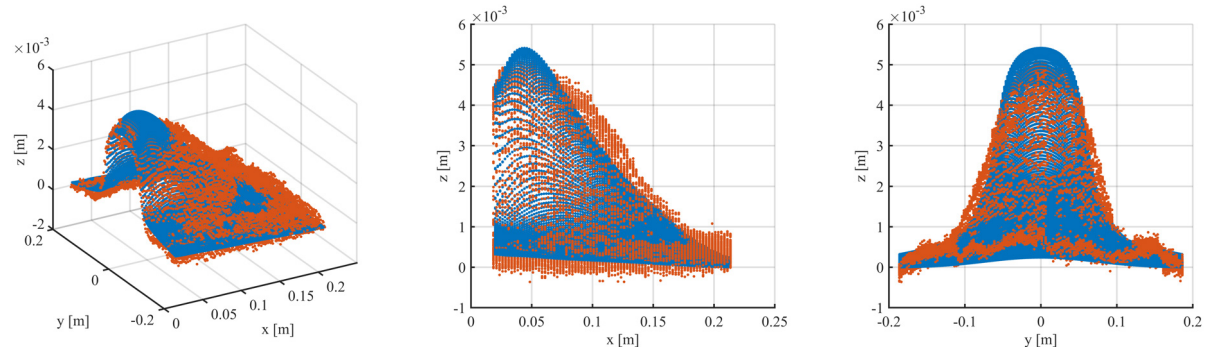

Fig. 9: Resulting soil deformation in SCM, shown in blue, and experimental result, shown in orange. With correctly set parameters Ψ_{Angle} and Ψ_{Distance} SCM shows a close match of the soil deformation.

With this identification procedure values Ψ_{Shape}, Ψ_{Angle} and Ψ_{Distance} were determined. These value are kept constant for all following experiments.

4.2 Single Wheel Experiment

To verify the selected parameters a single wheel scenario was selected. A wheel with a diameter of 0.5 m is moved with a slip ratio of 20 %. The resulting flow depth and flow velocity is then compared against PIV images. Keep in mind that, due to the discrete nature of SCM, no vertical variation in the soil flow is distinguishable.

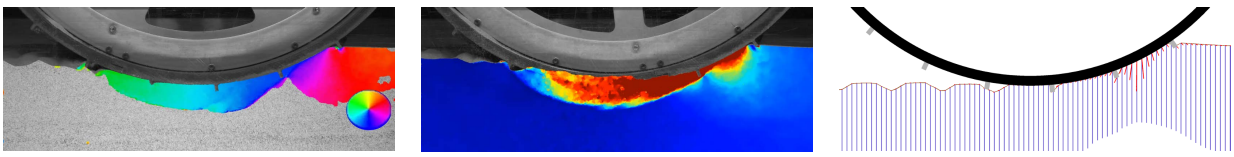

Fig. 10: Comparison between the flow measured with PIV and results generated by SCM. PIV images provided by NASA/JPL/Carnegie Mellon University.

Fig. 10 shows the comparison of the PIV measurements with color coded flow direction on the left, with color coded flow magnitude in the middle and the SCM results on the right. In the SCM results the purple area is used to visualize the flow depth and red is used to visulize the flow velocity.

When comparing the SCM results to the PIV data two important similarities can be identified. Firstly the point of the flow velocity reversing from flowing in driving direction to flowing backwards is at the same point. Both SCM and PIV data show a similar shape of failure with an extension to the front of the wheel as well as a soil

flowing backwards under the wheel. The visual difference of SCM showing a much larger area, is a result of SCM showing a binary representation of moving soil without any regard if the flow has a meaningful magnitude. The PIV data on the other hand is showing a continuous progression with a cut off if the flow velocity drops under 1 % of the highest observed. For a detailed explanation on the methodology used for the PIV data see [13, 14]. Nevertheless the flow velocity observed directly below the wheel seems to be too low in SCM.

4.3 Full rover system simulation

Since a quantitative validation of the resulting force is part of future work, this paper will only show a qualitative analysis of the effects observed in a full system simulation. A screen shot of this simulation is shown in Fig. 1. In the used scenario a four wheel rover is placed on flat terrain. After an initial settling period the wheels are rotated with a constant angular velocity of $2\,\mathrm{rad\,s^{-1}}$. The rover starts moving on the flat terrain and hits a15° slope after driving for roughly 1.5 m. The resulting slip of the full vehicle is then plotted over the driven distance in Fig. 11.

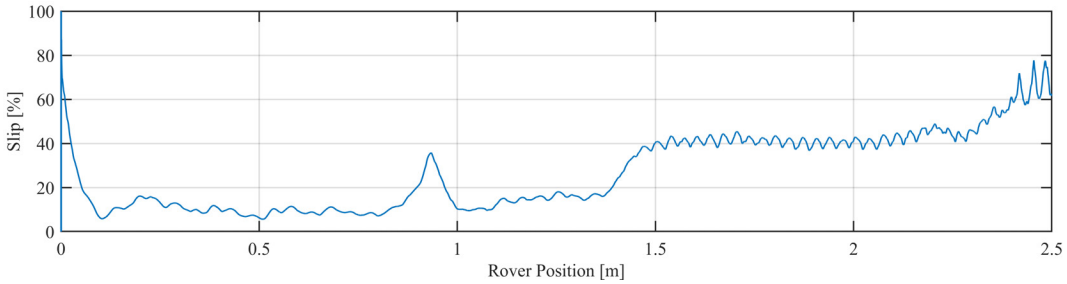

Fig. 11: Resulting rover slip in full rover simulation with SCM.

In the resulting slip important effects can be identified. For once, significant slip between 0.0 m to 0.2 m is necessary to accelerate the rover. Once a constant velocity is reached at 0.25 m a slip of roughly 10 % is needed to maintain this velocity. Secondly once the trailing wheels enter the rut of the leading wheels the slip at 0.9 m increases sharply due to the trailing wheels passing through the bump left from placing the front wheels. From 1 m to 1.3 m the trailing wheels drive in the rut left by the leading wheels, which leads to a slight increase in slip due to the multi pass effect. This effect is a result of the front wheels slightly loosening the soil and decreasing the traction capabilities of the trailing wheels. The slip increases at 1.2 m to 2 m once the front wheel starts driving uphill and approaches 80 % once all four wheels are on the slope at 2.4 m.

5 Conclusions

Concluding the presented approach for modeling the soil flow in SCM shows promising results. And does not increase the computational complexity significantly. The new approach has introduced three independent parameters describing the soil flow which can be identified for a sand in an experimental setup. The proposed assumptions to model the flow have verified in experiments. All three experiments indicate that the proposed algorithm does model the soil flow as well as the resulting deformation and effects correctly. The weighing functions used to infer a soil distribution are a current topic of research. Goal is to derive those from physical soil processes and directly relate the used parameters to measurable soil parameters. A validation campaign, in cooperation with JPL, comparing SCM single wheel experiments is currently in progress.

Acknowledgements

All PIV data used for this publication were kindly provided by NASA/JPL/Carnegie Mellon University.

References

[1] R. E. Arvidson, J. Bell, P. Bellutta, N. A. Cabrol, J. Catalano, J. Cohen, L. S. Crumpler, D. Des Marais, T. Estlin, W. Farrand, *et al.*, "Spirit mars rover mission: Overview and selected results from the northern home plate winter haven to the side of scamander crater," *Journal of Geophysical Research: Planets*, vol. 115, no. E7, 2010.

[2] R. E. Arvidson, K. D. Iagnemma, M. Maimone, A. A. Fraeman, F. Zhou, M. C. Heverly, P. Bellutta, D. Rubin, N. T. Stein, J. P. Grotzinger, *et al.*, "Mars science laboratory curiosity rover megaripple crossings up to sol 710 in gale crater," *Journal of Field Robotics*, vol. 34, no. 3, pp. 495–518, 2017.

[3] S. Michaud, M. Hoepflinger, T. Thueer, C. Lee, A. Krebs, B. Despont, A. Gibbesch, and L. Richter, "Lesson learned from exomars locomotion system test campaign," in *Proceedings of 10th Workshop on Advanced Space Technologies for Robotics and Automation, ESTEC The Netherlands*, 2008.

[4] F. Buse, T. Bellmann, R. Lichtenheldt, and R. Krenn, "The DLR Terramechanics Robotics Locomotion Lab," *ISAIRAS*, 2018.

[5] R. Lichtenheldt and B. Schäfer, "Locomotion on soft granular soils: A discrete element based approach for simulations in planetary exploration," in *12th Symposium on Advanced Space Technologies in Robotics and Automation: ASTRA 2013*, (Noordwijk, the Netherlands), 2013.

[6] B. Trease, R. Arvidson, R. Lindemann, K. Bennett, F. Zhou, K. Iagnemma, C. Senatore, and L. Van Dyke, "Dynamic modeling and soil mechanics for path planning of the mars exploration rovers," in *ASME 2011 International Design Engineering Technical Conferences and Computers and Information in Engineering Conference*, pp. 755–765, American Society of Mechanical Engineers, 2011.

[7] M. Hellerer, S. Barthelmes, and F. Buse, "The dlr rover simulation toolkit," 2017.

[8] G. Ishigami, A. Miwa, K. Nagatani, and K. Yoshida, "Terramechanics-based model for steering maneuver of planetary exploration rovers on loose soil," *Journal of Field robotics*, vol. 24, no. 3, pp. 233–250, 2007.

[9] A. Azimi, J. Kövecses, and J. Angeles, "Wheel–soil interaction model for rover simulation and analysis using elasto-plasticity theory," *IEEE Transactions on robotics*, vol. 29, no. 5, pp. 1271–1288, 2013.

[10] R. Krenn and G. Hirzinger, "SCM a Soil Contact Model for Multi-Body System Simulations," *Proceedings of the 11th European Regional Conference of the ISTVS 2009I, October 5-8, Bremen, Germany*, 2009.

[11] F. Buse, R. Lichtenheldt, and R. Krenn, "SCM-A novel approach for soil deformation in a modular soil contact model for multibody simulation," *IMSD2016 e-Proceedings*, 2016.

[12] K. Terzaghi, , *et al.*, *Soil Mechanics in Engineering Practice*, vol. 1. 1996.

[13] S. J. Moreland, *Traction Processes of Wheels in Lose, Granular Soil*. PhD thesis, Carnegie Mellon University, 2013.

[14] K. Skonieczny, S. J. Moreland, V. M. Asnani, C. M. Creager, H. Inotsume, and D. S. Wettergreen, "Visualizing and analyzing machine-soil interactions using computer vision," *Journal of Field Robotics*, vol. 31, no. 5, pp. 820–836, 2014.

[15] J. Y. Wong, *Theory of Ground Vehicles*. Hoboken, New Jersey, USA: John Wiley & Sons, Inc., 4 ed., 2008.